THE JOURNAL OF PHYSICAL CHEMISTRY A

Article

pubs.acs.org/JPCA

Theoretical Investigations of the Reactions of N- and O-Containing Species on a C(100):H 2 × 1 Reconstructed Diamond Surface

Mark W. Kelly,[†] Sarah C. Halliwell,[†] W. Jeff Rodgers,[†] Jason D. Pattle,[†] Jeremy N. Harvey,[*,‡] and Michael N. R. Ashfold[†,*]

[†]School of Chemistry, University of Bristol, Bristol BS8 1TS, U.K.

[‡]K.U. Leuven, Department of Chemistry, Celestijnenlaan 200F, B-3001 Heverlee, Belgium

Supporting Information

ABSTRACT: Quantum mechanical and hybrid quantum mechanical/molecular mechanical cluster models were used to investigate possible reaction mechanisms whereby gas-phase NH_x (x = 0−2), CNH_x (x = 0, 1), and OH radicals can add to, and incorporate in, a C−C dimer bond on the C(100):H 2 × 1 diamond surface during chemical vapor deposition (CVD) from microwave-activated C/H containing gas mixtures containing trace amounts of added N or O. Three N incorporation routes are identified, initiated by N, NH, and CN(H) addition to a surface radical site, whereas only OH addition was considered as the precursor to O incorporation. Each is shown to proceed via a ring-opening/ring-closing reaction mechanism analogous to that identified previously for the case of CH_3 addition (and CH_2 incorporation) in diamond growth from a pure C/H plasma. On the basis of the relative abundances of N atoms and NH radicals close to the growing diamond surface, the former is identified as the more probable carrier of the N atoms appearing in CVD grown diamond, but fast H-shifting reactions postaddition encourage the view that NH is the more probable migrating and incorporating species. CN radical addition is deemed less probable but remains an intriguing prospect, since, if the ring-closed structure is reached, this mechanism has the effect of adding two heavy atoms, with the N atom sitting above the current growth layer and thus offering a potential nucleation site for next-layer growth.

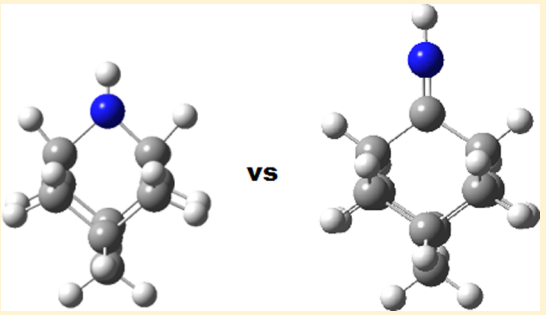

1. INTRODUCTION

Modeling has played a key role in determining the feasibility and mechanisms of reactions whereby reactive gas-phase species incorporate into a growing diamond film during chemical vapor deposition (CVD).[1−14] Typical gas mixtures for growing high-quality diamond films contain 1−5% CH_4 in H_2, and the methyl (CH_3) radical is now generally considered to be the main species responsible for diamond growth from activated C/H gas mixtures. Spatially resolved laser absorption studies of the diamond-growing plasma along with complementary plasma modeling confirm CH_3 as the most abundant carbon containing radical species immediately above the growing diamond surface,[15] and theoretical studies have identified energetically favorable reaction sequences whereby a CH_3 species can bind to a surface radical site, incorporate into the surface as a CH_2 group and, if necessary, migrate to a step edge.[12] Analogous reaction sequences have been demonstrated for the case of B atom and/or BH radical addition to the surface of CVD diamond grown from C/H gas mixtures containing trace quantities of B_2H_6.[16,17]

Addition of trace amounts (20 ppm or less) of N_2 to microwave-activated C/H gas mixtures has been shown to enhance diamond growth rates and favor formation of the C(100):H 2 × 1 reconstructed diamond surface.[18−28] Several theoretical studies have sought to explain these observations. For example, Larsson and co-workers investigated the effect of coadsorbed NH species on the binding of CH_3/CH_2 species at different step edges on the H-terminated diamond (100)−2 × 1 surface[29] and the effects of substitutional N atoms on the energetics (and thus the rates) of the elementary reactions involved in incorporating an incident gas-phase CH_3 radical on the growing diamond surface.[30−32] These studies concluded that the extra electron density provided by a near-surface N atom has the effect of weakening proximal surface C−H bonds, thereby enhancing the rate of the H-abstraction step that creates the surface radical site necessary for CH_3 radical addition.[32] Butler and Oleynik[33] focused attention on the CN radicals present in a C/N/H plasma and showed how CN adsorption on a diamond (111) surface might act as a renucleation site for the growth of a new layer. Most recent interest in CVD growth from C/N/H gas mixtures on (111)-oriented diamond substrates has focused on the finding that the spontaneously generated nitrogen-vacancy (NV) defects are highly oriented along the [111] axis.[34−36] These findings have been rationalized by atomistic simulations that assume addition of a gas-phase N atom to C(111) growing laterally in step-flow

Received: January 16, 2017
Revised: February 15, 2017
Published: February 16, 2017

DOI: 10.1021/acs.jpca.7b00466
J. Phys. Chem. A 2017, 121, 2046−2055

mode,[37] though another recent study suggests that a high alignment of NV defects along the [111] axis could also be obtained by thermal annealing if the sample is under an appropriate biaxial compressive strain.[38]

Oxygen is another species often found in gas mixtures used for diamond CVD,[39] either as part of any (trace) air impurity or, in higher abundances, when used as a deliberate constituent (e.g., CO and CO_2) within the source gas.[40] Combined spatially resolved laser diagnosis and modeling studies of microwave-activated 35%(CH_4)/35%(CO_2)/30%(H_2) gas mixtures operating at a total pressure p = 150 torr and input power P = 1 kW identified OH and HCO as the most abundant O-containing radical species in the hot plasma region ($T_{gas} \approx 2900$ K) but suggested that the OH densities close to the growing diamond surface were only ~0.2% that of the CH_3 radical[41,42]—consistent with the paucity of data relating to O doping levels in CVD diamond samples.

Much of the recent activity has sought to explore how pre-existing nitrogen in a diamond sample affects further growth by CVD on that sample, whereas the primary aim of the present study is to provide a better understanding of the gas-surface chemistry by which the nitrogen is initially incorporated. To this end, we used quantum mechanical (QM) and hybrid QM-molecular mechanics (MM) cluster models to investigate the energetics, and thus the feasibility, of elementary reaction sequences whereby potential reactive species (N, NH, CN, etc) might add to, and incorporate in, a C(100):H 2 × 1 diamond surface. Combining the results of these calculations with knowledge of the near-surface relative number densities gained from companion laser diagnostics and plasma modeling studies[43] indicates that the most abundant, potentially reactive, nitrogen-containing species impacting on the growing diamond surface during CVD is likely to be process condition-dependent. N atoms are deduced to be dominant under the conditions used in our laboratory ($p \approx 150$ torr, $P \approx 1.5$ kW), but CN radicals are seen to gain in relative abundance at higher p and/or P. Gas-surface reaction sequences starting with addition of an OH radical to a diamond surface radical site are reported also, and similarities and differences with the corresponding NH_x (x = 0−2) reaction pathways are highlighted.

2. COMPUTATIONAL DETAILS

The present QM and QM/MM calculations followed closely the methodologies used in our previous studies of BH_x (x = 0−2) and CH_x (x = 0−3) radical addition to, and migration on, a C(100):H 2 × 1 surface.[12,13,16,44,45]

The QM calculations used density functional theory (DFT) and, in most cases, the small C_9H_{14} cluster shown in Figure 1 to mimic the C−C surface dimer bond. Potential energy minima and transition states (TSs) associated with accommodation of N, NH, NH_2, CN, HCN, HNC, and OH species were calculated with the B3LYP functional and the 6-31G(d) basis set within Gaussian 09.[46] Calculating the vibrational frequencies allowed confirmation that a given stationary point was indeed a TS and estimation of the zero-point energy (ZPE) correction. Single-point energies were then recalculated using the larger 6-311G(d,p) basis set and corrected by the ZPE to yield the reported energies, quoted in kilojoules per mole.

The same reaction sequences were investigated using QM/MM methods using the QoMMMa program.[47,48] These calculations employed the same C_9 cluster (calculated using Jaguar 5.0[49]) embedded in an extended array of C atoms arranged in a 12 layer thick slab, with initial positions defined by the bulk diamond lattice points and a 2 × 1 reconstructed surface comprising a 5 × 9 array of C−C dimer bonds, modeled with TINKER.[50] The peripheral atoms

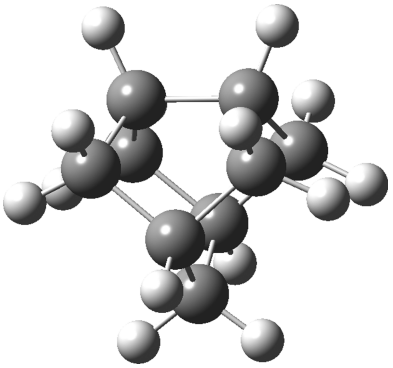

Figure 1. C_9H_{14} cluster used as the model for a C−C dimer bond on the C(100):H 2 × 1 surface.

(with nonchemical stoichiometry) were held fixed during these calculations. As before,[44] the QM region was described using the B3LYP functional with the 6-31G(d) basis set, the MM region was treated with the MM2 protocol, and the coupling between the two regions was described using nonbonded Lennard-Jones terms together with hydrogen link atoms to saturate valences in the QM region. More accurate single-point QM energies were then recalculated at the optimized geometries (using the B3LYP functional and a 6-311G(d,p) basis set) and added to the MM energy and the QM/MM nonbonded interaction contribution to yield the final QM/MM energy. Approximate TSs were identified by calculating the energy of the system at successive values along a chosen reaction coordinate R using a harmonic constraint to hold the system close to the required value and allowing the structure to relax in all other degrees of freedom; the energy of the TS was taken as the maximum along the curve obtained by plotting the single-point QM/MM energy versus R. The single-point QM/MM energies reported for the intermediate, final, and transition states are all quoted in kilojoules per mole (after inserting a correction for ZPE effects taken from the QM calculations) relative to that of the initial reactants, which define E = 0. All QM structures and energies are reported in the Supporting Information. A sample TS structure derived from the QM/MM calculations is also reported in the Supporting Information.

Species migration post-chemisorption was not investigated in as much detail as in our earlier studies of CH_2[44] and BH[45] additions and migration, but the present work includes a preliminary QM/MM study of NH incorporation at a single layer type-B step edge (i.e., a one-layer high step in which the C−C bonds on the upper {100} terrace are aligned parallel to the step edge). This particular study employed a larger QM region involving 23 carbon atoms, and the reported energies in this case are not zero-point corrected. The initial and final structures in the migration pathway both contain two radical sites (i.e., two unpaired electrons); their minimum-energy forms will have triplet electronic configurations. The minimum-energy form of the ring closed intermediate, in contrast, is a singlet spin state, which was calculated using restricted DFT, whereas unrestricted DFT methods were used for the open-shell species.

3. RESULTS

The various elementary reaction sequences explored in this work with both QM and QM/MM methods are reported in turn. We note that we previously used a similar computational strategy, with QM calculations on a relatively small model, and QM/MM calculations with a QM region of similar size to that used in the QM calculations. Test calculations (see, e.g., ref 12) suggest that the results described here should be of sufficient accuracy for the present purposes.

3.1. Addition of NH_x (x = 0−2) Species to a C(100):H 2 × 1 Surface. Figure 2 shows the energetics (calculated using the small QM cluster) of reaction sequences wherein NH_x (x =

DOI: 10.1021/acs.jpca.7b00466
J. Phys. Chem. A 2017, 121, 2046−2055

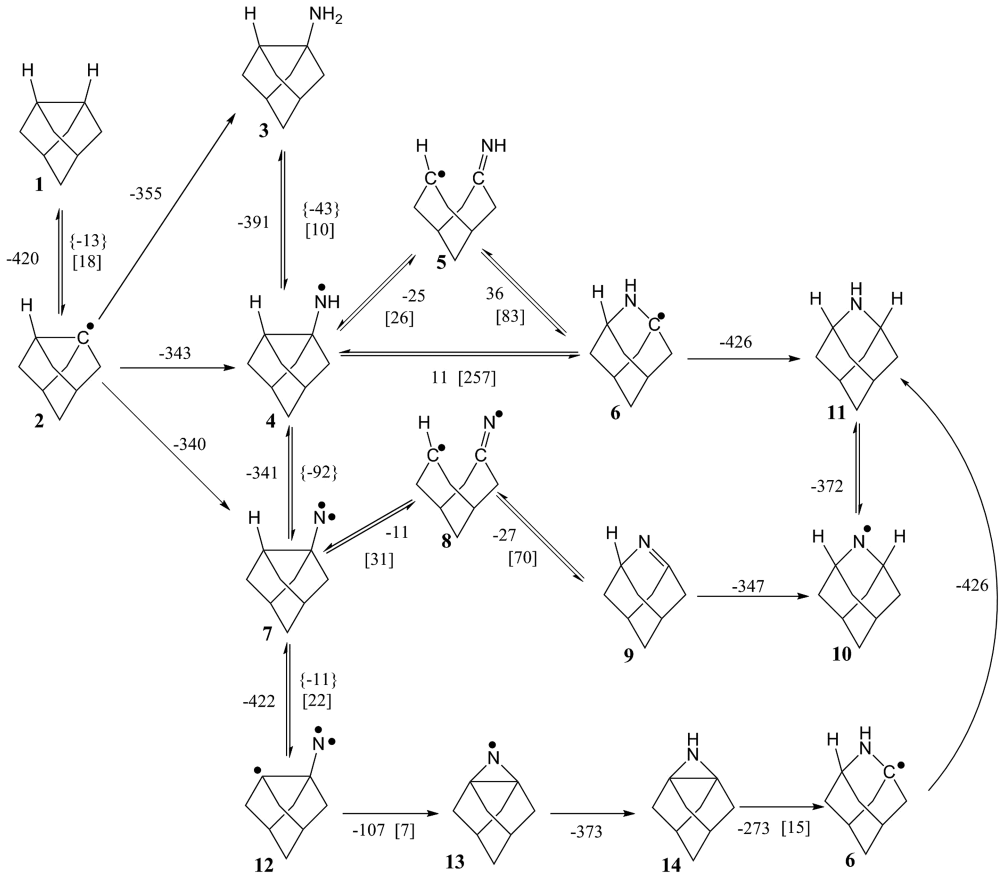

Figure 2. Reaction pathways calculated for the incorporation of NH_x species onto the C(100):H 2 × 1 surface calculated using QM, B3LYP, with a 6-311G(d,p) basis set. The structures are labeled with numbers to their bottom left. For compactness, activation energies E_a and the enthalpies of H atom abstraction reactions of the form RH + H → R + H_2 are shown, in kilojoules per mole, using square [ ] and curly { } brackets, respectively; all other reaction enthalpies are shown without brackets.

0−2) adsorption to a C−C dimer bond can lead to eventual accommodation as a bridging NH group. Surface activation, as usual, involves removal of a terminating H atom by reaction with an incident gas-phase H atom (step **1**→**2**, characterized by a reaction enthalpy ΔE = −13 kJ mol^{-1} and an activation energy E_a = 18 kJ mol^{-1}). The subsequent adsorption of a gas-phase NH_2, NH, or N species at the surface radical site is, in each case, exothermic—yielding structures **3**, **4**, and **7**—and the energy barriers associated with the H abstraction reactions that enable interchange between these structures are small (E_a = 10 kJ mol^{-1} for conversion of **3** to **4**, and essentially no barrier for the conversion **4**→**7**). The NH_2 adduct is unreactive unless activated by an H abstraction reaction (or H addition and loss as NH_3), whereas the open shell adducts **4** and **7** can undergo further reactions that could lead to N incorporation at the diamond surface.

The reaction sequence leading to NH incorporation is analogous to the ring-opening, ring-closing mechanism reported previously for the case of CH_2 incorporation.[7,14] Ring opening (**4**→**5**) is exothermic, with a low barrier (ΔE = −25 kJ mol^{-1}, E_a = 26 kJ mol^{-1}). The ring-closing step (**5**→**6**) is endothermic and involves a larger barrier (ΔE = 36 kJ mol^{-1}, E_a = 83 kJ mol^{-1}). As noted previously,[14] barriers typically need to exceed 100 kJ mol^{-1} before they become a significant impediment to surface rearrangement reactions at the typical substrate temperatures (T_{sub} = 1100−1200 K) prevailing during diamond CVD. The rival concerted rearrangement **4**→**6** is calculated to involve a prohibitively large barrier (E_a = 257 kJ mol^{-1}). A final, exothermic, H atom addition at the surface radical site in structure **6** completes the incorporation of NH (structure **11**). The reaction sequence **1**→**2**→**4** → **5**→**6**→**11** was also investigated by QM/MM methods. The resulting potential-energy profile is shown in Figure 3. The ring-closing step **5**→**6** is here found to be exothermic and to involve a larger

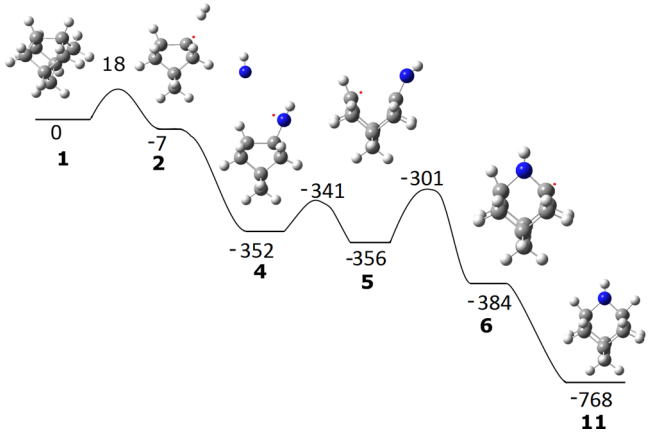

Figure 3. Energy profiles for addition of a ground-state NH radical to, and incorporation in, a C−C dimer bond on the C(100):H 2 × 1 surface calculated using QM/MM, B3LYP, 6-311G(d,p): MM2. Energies are quoted in kilojoules per mole defined relative to structure **1**, and the displayed structures include the hydrogen link atoms.

DOI: 10.1021/acs.jpca.7b00466
J. Phys. Chem. A 2017, 121, 2046−2055

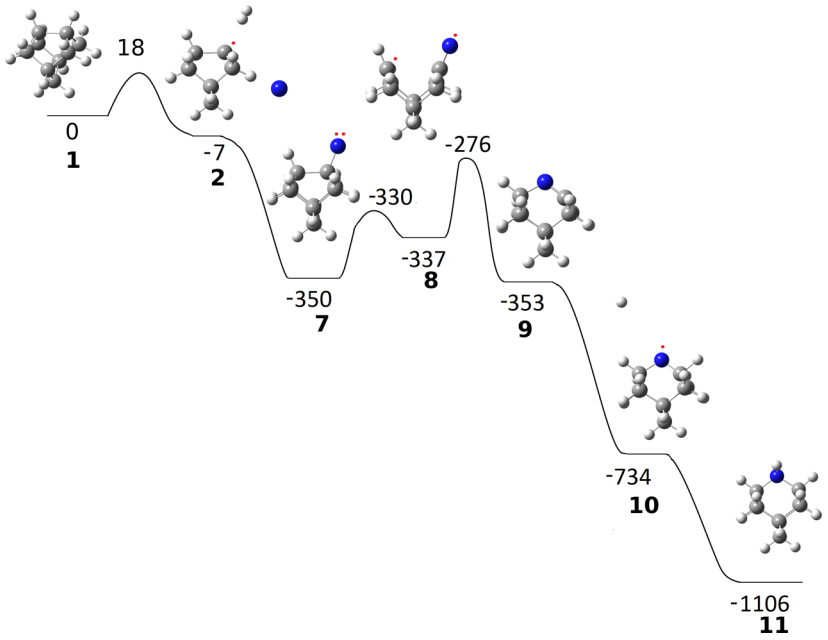

Figure 4. Energy profiles for addition of a ground-state N atom to and eventual incorporation as a bridging NH group between two C atoms originally linked by a C−C dimer bond on the C(100):H 2 × 1 surface, calculated using QM/MM, B3LYP, 6-311G(d,p): MM2. Energies are quoted in kilojoules per mole defined relative to structure **1**, and the displayed structures include the hydrogen link atoms.

energy barrier (ΔE = −28 kJ mol^{-1}, E_a = 55 kJ mol^{-1}) than the ring-opening step **4**→**5** that necessarily precedes it.

The reaction sequence starting from addition of a ground-state N atom involves a change in ground-state spin multiplicity; structures **7** and **8** were calculated as triplet spin states, but the ground state of the ring-closed structure **9** is a closed-shell singlet (and calculated as such). As in the case of CH_2 migration,[44] we find that the singlet and triplet states of the diradical **8** are close in energy and thus assume that the interchange between spin states in reactions at the diamond surface will not be rate limiting and that the transformation from **8** to **9** can proceed on whichever potential energy surface (PES) presents the lower energy barrier (i.e., the singlet PES). Given that caveat, the QM calculations (Figure 2) find both the initial ring-opening (**7**→**8**, both calculated as triplets) and subsequent ring-closing (**8**→**9**, with **8** now treated as a singlet) steps to be exothermic (ΔE = −11 kJ mol^{-1} and −27 kJ mol^{-1}, respectively). The latter step has the larger associated energy barrier (E_a = 70 kJ mol^{-1}). Given the relatively facile nature of the indirect transformation, in this case, we did not try to locate a pathway for a concerted rearrangement **7**→**9**, though it is possible that this alternative route exists.

Subsequent (exothermic) additions of two H atoms from the gas phase leads through the radical structure **10** to yield the same final structure **11** wherein an NH group bridges the atoms involved in the original C−C dimer bond. As Figure 4 shows, the QM/MM calculated energy profile for the reaction sequence **1**→**2**→**7** → **8**→**9** → **10**→**11** accords well with the QM data shown in Figure 2, with the QM/MM calculations suggesting slightly lower energy barriers for the ring-opening (**7**→**8**) and ring-closing (**8**→**9**) steps (E_a = 20 and 61 kJ mol^{-1}, respectively).

As noted previously, H atom abstraction and addition reactions involving the pendant NH_x (x = 0−2) group will ensure a dynamic equilibrium between structures **3**, **4**, and **7**. However, only N and NH (i.e., NH_x species with one or more nonbonding electrons) can initiate ring-opening (i.e., step **4**→**5** or **7**→**8**). Relative to the QM/MM calculations, the QM cluster calculations predict a greater exothermicity for these C−C bond-breaking/C═N double bond-forming steps. They also predict larger barriers for the subsequent ring-closing step (i.e., **5**→**6** and **8**→**9**). Both of these trends can be attributed to the effect of the surrounding MM network, which limits the separation between the two C atoms to ∼2.5 Å during geometry optimization (cf. ∼2.9 Å in the QM calculations with the bare C_9 cluster and ∼2.3 Å in the subsequent ring-closed structures **6** or **9**).

NH migration on the C(100):H 2 × 1 reconstructed diamond surface was not investigated extensively, but Figure 5 shows initial QM/MM results for the specific case of NH incorporation at a one-layer high step in which the C−C bonds on the upper {100} terrace are aligned parallel to the step edge. This sequence starts with structure (a), with a pendant NH

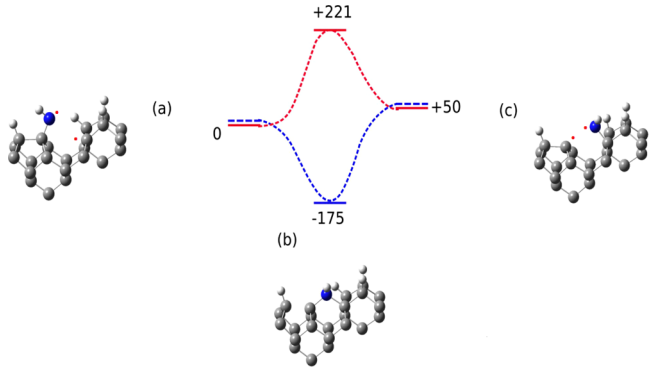

Figure 5. Singlet (blue) and triplet (red) energy profiles for NH migration between two C(100):H 2 × 1 surfaces separated by a single-layer S_B step edge. Energies (B3LYP QM/MM, 6-311G(d,p): MM2) are quoted in units of kilojoules per mole defined relative to structure (a). To avoid congestion, the hydrogen link atoms were omitted from the displayed structures.

DOI: 10.1021/acs.jpca.7b00466
J. Phys. Chem. A 2017, 121, 2046−2055

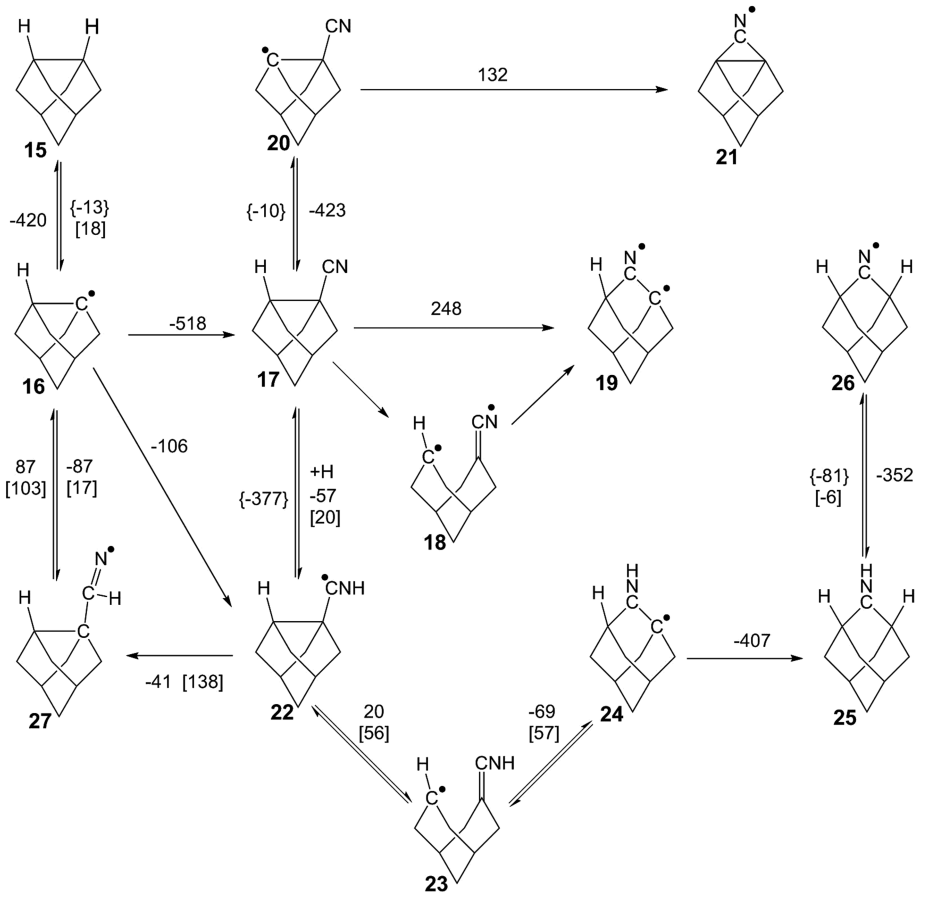

Figure 6. Reaction pathways calculated for the incorporation of CN(CNH) species onto the C(100):H 2 × 1 surface calculated using QM, B3LYP, 6-311G(d,p). The structures are labeled with numbers to their bottom left and, for compactness, activation energies E_a and the enthalpies of H atom abstraction reactions of the form RH + H → R + H_2 are shown, in kilojoules per mole, using square [ ] and curly { } brackets, respectively; all other reaction enthalpies are shown without brackets.

bonded to a C atom on the lower terrace and a surface radical site on a neighboring C atom on the upper terrace. The positions of the NH and the radical site are reversed in structure (c). Both (a) and (c) are biradicals with triplet minimum-energy structures, whereas, as Figure 5 shows, the minimum-energy structure of the six-membered ring-closed intermediate (b) is a singlet spin state. Thus, as in the cases of CH_2 and BH migration on the C(100):H 2 × 1 surface, NH accommodation (and the extension of step-flow growth) at such a step edge requires a spin-flip to access the deep (E = −175 kJ mol^{-1}) potential minimum associated with structure (b). Though a credible trap, we note that the depth of this well is less than those returned by equivalent calculations for BH and CH_2 incorporation at the same step edge.[44,45]

3.2. Addition of CN(H) to a C(100):H 2 × 1 Surface.

Figure 6 shows reaction sequences investigated by QM methods as possible routes to N incorporation following CN addition (**16**→**17**) to a surface radical site formed by the usual H abstraction reaction (**15**→**16**). The traditional ring-opening/ring-closing pathway (**17**→**18**→**19**), and its concerted analogue (**17**→**19**), can both be ruled out, as the overall process is prohibitively endothermic; furthermore, putative species **18** does not seem to be a stable point on the singlet or triplet PESs. H atom abstraction from **17** by an incident gas-phase H atom (**17**→**20**) is roughly thermoneutral (though entropically disfavored). Rearrangement of the resulting radical to the strained bridged structure **21** is again endothermic, and we do not consider this path further.

H addition to the preadsorbed CN (**17**→**22**) yields a structure with a pendant CNH group. As Figure 6 shows, direct addition of HNC to the surface radical site (**16**→**22**) is calculated as an alternative (exothermic) route to this intermediate, but the relative stabilities of HCN and HNC imply negligible gas-phase concentrations of the latter. The QM calculations identify several "unimolecular" decay pathways for **22** of which H atom desorption (**22**→**17**) is likely to have the highest rate constant. Isomerization of the pendant CNH group (**22**→**27**) and subsequent HCN desorption (**27**→**16**) can be ignored, given the calculated activation barrier for the first of these steps. The pendant CNH group has the necessary partially filled orbital to support ring-opening/ring-closing (**22**→**23**→**24**); however, the calculated barriers for these steps (E_a = 56 and 57 kJ mol^{-1}, respectively) are similar to that for H atom desorption. H atom addition (**24**→**25**) yields the final structure, wherein the original C−C dimer bond has now been replaced by a bridge comprising two heavy atoms (rather than one as in the case of CH_2 or NH incorporation). **25** can be activated by H atom abstraction (**25**→**26**), which constitutes a possible nucleation site for growth on the next layer.

The reaction sequence for possible CN(H) incorporation (i.e., **15**→**16**→**17** → **22**→**23** → **24**→**25**) was also investigated by QM/MM methods. Figure 7 displays the resulting energy

DOI: 10.1021/acs.jpca.7b00466
J. Phys. Chem. A 2017, 121, 2046−2055

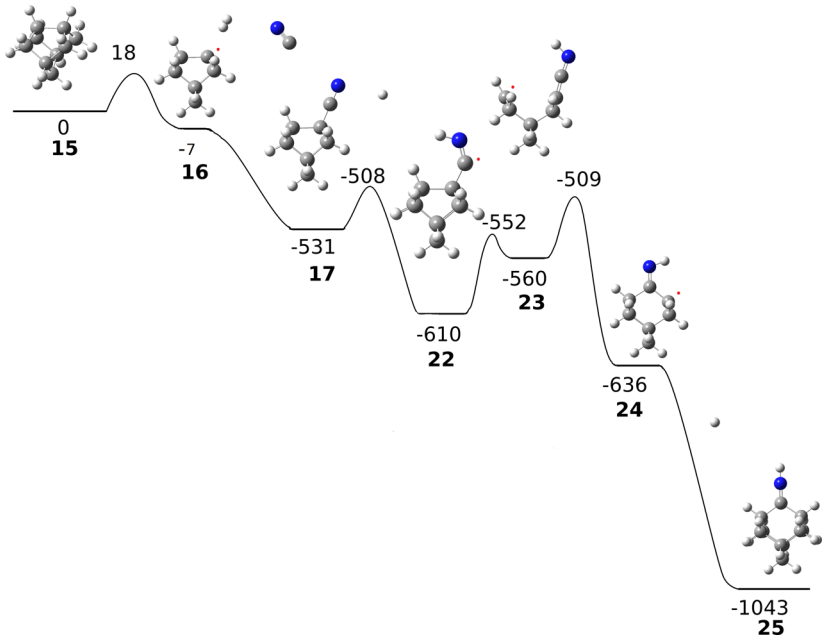

Figure 7. Energy profiles for successive addition of a CN radical and an H atom, and eventual incorporation as a bridging CNH group between two C atoms originally linked by a C−C dimer bond on the C(100):H 2 × 1 surface, calculated using QM/MM, B3LYP, 6-311G(d,p): MM2. Energies are quoted in kilojoules per mole defined relative to structure **15**, and the displayed structures include the hydrogen link atoms.

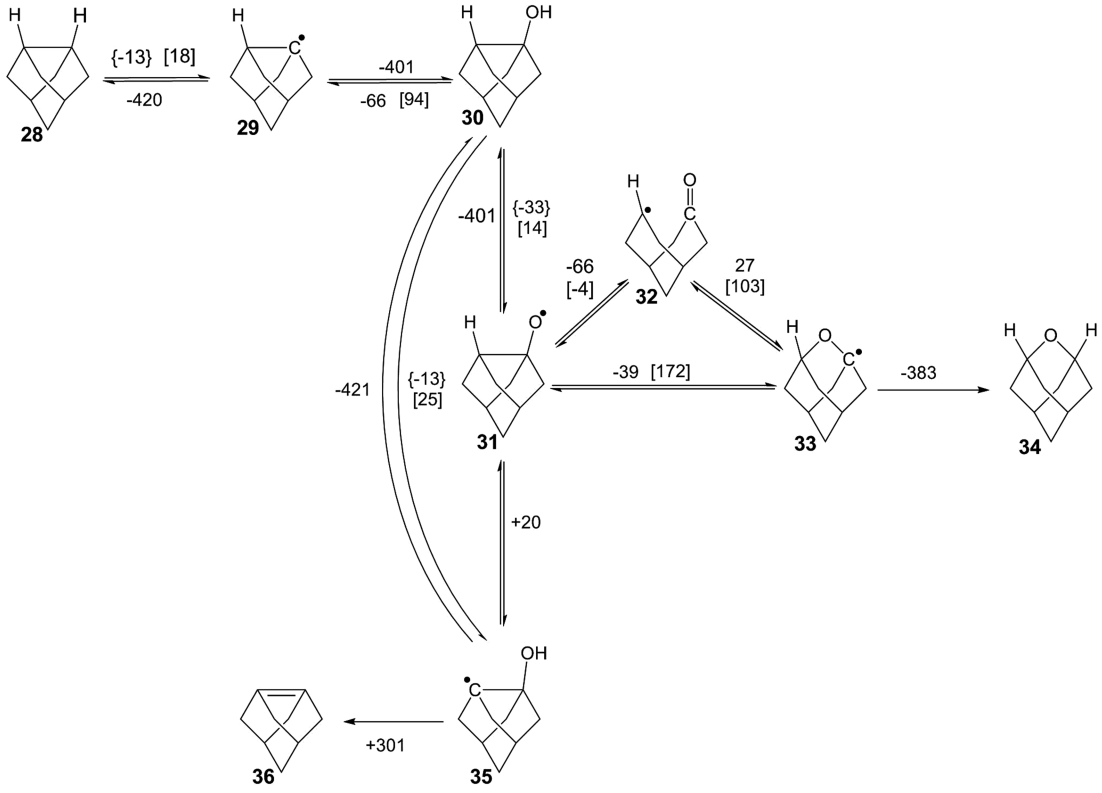

Figure 8. Reaction pathways calculated for the addition of an OH radical to the C(100):H 2 × 1 surface and eventual incorporation as a bridging O atom calculated using QM, B3LYP, 6-311G(d,p). The structures are labeled with numbers to their bottom left and, for compactness, activation energies E_a and the enthalpies of H atom abstraction reactions of the form RH + H → R + H_2 are shown, in kilojoules per mole, using square [ ] and curly { } brackets, respectively; all other reaction enthalpies are shown without brackets.

profile, which is reassuringly similar to that returned by the QM calculations. The QM/MM calculations find C−C bond cleavage to be more endothermic but still return energy barriers of less than 60 kJ mol^{-1} for both the ring-opening (**22**→**23**) and ring-closing (**23**→**24**) processes. Given the paucity of credible reaction pathways from **17**, we envisage that **17** and **22** are in dynamic equilibrium and that the sequence **22**→**23**→**24**→**25** should constitute a route to incorporating

DOI: 10.1021/acs.jpca.7b00466
J. Phys. Chem. A 2017, 121, 2046−2055

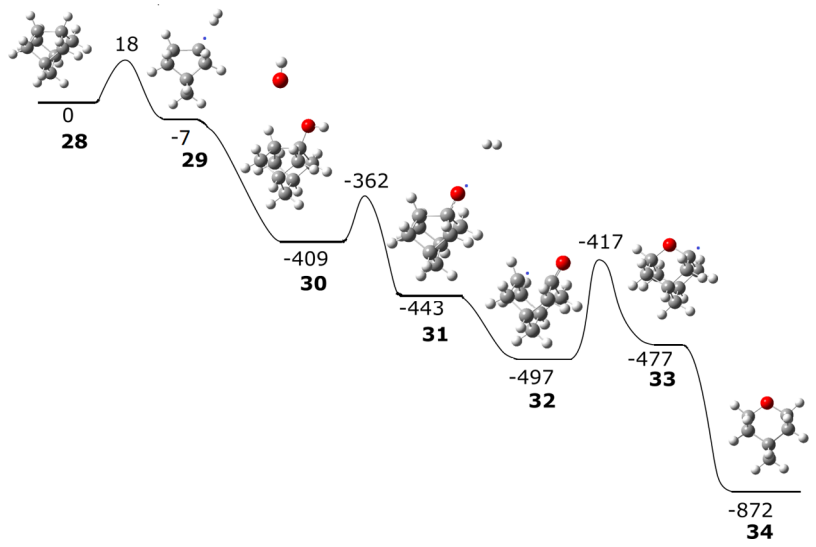

Figure 9. Energy profiles for the addition of OH and eventual incorporation as a bridging ether linkage between two C atoms originally linked by a C−C dimer bond on the C(100):H 2 × 1 surface, calculated using QM/MM, B3LYP, 6-311G(d,p): MM2. Energies are quoted in kilojoules per mole defined relative to structure **29**, and the displayed structures include the hydrogen link atoms.

CN radicals (with an efficiency that depends on the stability of **22** with respect to desorbing an H atom).

3.3. Addition of OH to a C(100):H 2 × 1 Surface. The OH radical is isoelectronic with NH_2, and CH_3 and has previously been shown to be the more abundant OH_x (x = 0,1) species near the growing diamond surface in a microwave-activated C/O/H plasma. Given their relative abundances, the initiating H atom abstraction will generally involve an incident gas-phase H atom (**28**→**29** in Figure 8) rather than an OH radical. For completeness, however, we note that the corresponding H atom abstraction by an incident OH radical is calculated to be barrierless and exothermic (ΔE = −47 kJ mol^{-1})—reflecting the greater relative strength of the O−H (cf. C−H) bond.

Figure 8 shows possible reaction pathways leading to O incorporation calculated using QM, B3LYP, with a 6-311G-(d,p) basis set. As noted previously,[51] an OH radical will readily bind to a surface radical site (**29**→**30**). Loss of this pendant OH by H atom addition and desorption as H_2O (**30**→**29**) is restricted by the much larger activation barrier (E_a = 94 kJ mol^{-1}) than those for H abstraction from the hydroxyl group (**30**→**31**, E_a = 14 kJ mol^{-1}) or the neighboring C atom (**30**→**35**, E_a = 25 kJ mol^{-1})—both of which abstraction reactions are calculated to be mildly exothermic. Intermediate **31** supports the necessary odd-electron to initiate ring opening (**31**→**32**), which is found to be exothermic (ΔE = −66 kJ mol^{-1}) and effectively barrierless. (We find a small (4 kJ mol^{-1}) barrier at the B3LYP/6-31(d) level of theory, but this vanishes after applying the zero-point energy correction.) The subsequent ring closing (**32**→**33**) is calculated to be endothermic with a significant barrier (ΔE = 27 kJ mol^{-1}, E_a = 103 kJ mol^{-1})—albeit smaller than the barrier associated with the alternative concerted pathway **31**→**33**. Addition of one further H atom (**33**→**34**) leads to the bridging ether linkage identified in previous theoretical studies of oxygenated diamond (100) surfaces.[51−53] Oxygen is not generally viewed as a significant contaminant in CVD-grown diamond, but the present study failed to identify any obvious low-energy O loss mechanisms following formation of the adduct **30**. Prior thermal desorption studies[54,55] suggest the existence of relatively low-energy pathways leading to loss of stable species like CO, but these have not been investigated here. As noted previously, H addition followed by H_2O desorption (**30**→**29**) is limited by a significant barrier, while the possible elimination of OH or H_2O accompanying rearrangements **35**→**36** or **30**→**36** are prohibitively endothermic.

The energy profile for the OH addition and O incorporation steps found using QM/MM methods reproduces the QM results well, as shown in Figure 9. The QM/MM calculations also find no barrier to ring-opening (**31**→**32**)—reflecting the stability of the open carbonyl structure—and return similar values for the exothermicity of the ring-opening step (ΔE = −54 kJ mol^{-1}) and the endothermicity of the subsequent ring-closure (**32**→**33**, ΔE = 20 kJ mol^{-1}, E_a = 80 kJ mol^{-1}). As in the case of NH incorporation, the small changes in energetics with respect to the QM calculations can be attributed to the extended MM network of C atoms constraining the separation of the C atoms previously linked by the dimer bond in structure **32**.

■ DISCUSSION

The present study of NH, CN(H) and O incorporation into a C−C dimer bond on a C(100):H 2 × 1 surface complements and extends our previous studies of CH_2[12,44] and BH[45] incorporation on such a surface. As in these previous examples, sequential (and/or concerted) ring-opening/ring-closing pathways constitute the lowest-energy routes to inserting bridging NH, CNH, or O species between two carbon atoms that were previously linked by a dimer bond. Comparisons of the relative energetics for the isoelectronic species CH_2, NH, and O are informative. In order, the QM/MM calculations show the ring-opening step becoming increasingly exothermic (ΔE = +28,[12] −4, and −54 kJ mol^{-1}), while the barrier to ring-opening declines (E_a = +44[12] and +10 kJ mol^{-1} for CH_2 and NH, respectively, while ring-opening in the case of O incorporation is calculated to be barrierless). The calculated energetics for the ring-closing step show the opposite trend, switching from exothermic to endothermic (ΔE = −78, −28, and +20 kJ mol^{-1}) and displaying progressively larger activation barriers (E_a = 45, 55, and 80 kJ mol^{-1}). These trends can all be traced to

DOI: 10.1021/acs.jpca.7b00466
J. Phys. Chem. A 2017, 121, 2046−2055

the different relative stabilities of the respective ring-opened structures: the ring-opened ketone structure is calculated to be a global minimum in the ring-opening/ring-closing sequence **31→32→33** (consistent with earlier theoretical conclusions regarding the relative stabilities of the ketone and ether structures[56] and temperature-dependent electron energy loss spectroscopy studies of the O-adsorbed diamond (100) surface[55]), whereas the adsorbed NH and CH_2 species prefer to exist in a ring-closed structure.

The deduced (small) energetic preference for the ring-opened (ketone) rather than the ring-closed (ether) form in the specific case of OH_x (x = 0,1) additions may be a contributory factor to the paucity of data relating to O defects in CVD diamond, since ring-closure is a necessary step in both the incorporation and migration of species on the diamond surface. Given the relative stability of the ketone (cf. ether) structure, adsorbed O atoms will spend a greater fraction of their time in the ring-open structure, wherein they may be more prone to further hydrogenation (by incident gas-phase H atoms) and/or to desorption (as CO).

The present calculations identify three ways in which N may incorporate at the (100):H 2 × 1 diamond surface—via N, NH, and CN(H) addition to a surface radical site. N and NH can both adsorb onto surface radical sites. The former are more abundant close to the growing diamond surface,[43] but, given the efficiency of the H-shifting reactions, NH is viewed as the more probable migrating species which—as Figure 5 shows—can incorporate at a single-atom step edge. Subsequent H abstraction (by reaction with a gas-phase H atom) and further C additions could then lead to the subsurface N atom that has been suggested as one possible route to catalyzing diamond growth.[32]

N incorporation via CN addition on the C(100):H 2 × 1 surface is deemed less probable for several reasons. First, the density of gas-phase CN radicals adjacent to the growing surface in the microwave-activated C/N/H gas mixtures used for diamond CVD is typically less than that of N atoms, though this imbalance is reduced when operating at higher pressures and/or microwave powers.[43] Second, as Figure 6 shows, the adsorbed CN species requires another gas-surface reaction step (an H atom addition) to form a CNH species (isoelectronic with CO) that is capable of promoting an energetically feasible ring-opening/ring-closing reaction sequence **22→23→24**. Third, the N−H bond in the CNH adduct is weak, and the binding energy of the CNH adduct (ΔE = 105 kJ mol^{-1}) is itself quite low, rendering this species prone to thermal dissociation (**22→17**) and/or desorption (**22→16**). Nonetheless, the possible incorporation of a CNH species remains an intriguing prospect since, if the ring-closed structure is reached, this mechanism alone has the effect of adding two heavy atoms, with the N atom sitting one layer above that of the current growth layer. This could serve to nucleate growth of a new layer and (given that this is generally seen as the rate-limiting step in diamond growth) thereby lead to an enhanced material growth rate.

■ ASSOCIATED CONTENT

Supporting Information

The Supporting Information is available free of charge on the ACS Publications website at DOI: 10.1021/acs.jpca.7b00466.

Cartesian coordinates and calculated energies are listed for all species involved in the QM calculations of Figures 2, 6, and 8 (PDF)

■ AUTHOR INFORMATION

Corresponding Authors

*E-mail: mike.ashfold@bris.ac.uk. (M.A.)
*E-mail: jeremy.harvey@kuleuven.be. (J.H.)

ORCID

Jeremy N. Harvey: 0000-0002-1728-1596
Michael N. R. Ashfold: 0000-0001-5762-7048

Notes

The authors declare no competing financial interest.
These data, and a sample structure for the full QM/MM system (in Tinker MM format) have also been stored in the Univ. of Bristol research data repository and are also openly available under the DOI: 10.5523/bris.2ddiq4srpok6o2aj83xl58jggx at https://data.bris.ac.uk/data/dataset/2ddiq4srpok6o2aj83xl58jggx.

■ ACKNOWLEDGMENTS

Financial support from the Engineering and Physical Sciences Research Council (Grant Nos. EP/H043292/1 and EP/K018388/1) and from Element Six Ltd is gratefully acknowledged. The authors are grateful to Dr. Y. Mankelevich (Moscow State Univ.) for many helpful discussions.

■ REFERENCES

(1) Harris, S. J. Mechanism for Diamond Growth from Methyl Radicals. *Appl. Phys. Lett.* **1990**, *56*, 2298−2300.
(2) Garrison, B. J.; Dawnkaski, E. J.; Srivastava, D.; Brenner, D. W. Molecular Dynamics Simulations of Dimer Opening on a Diamond (001) (2 × 1) Surface. *Science* **1992**, *255*, 835−8.
(3) Harris, S. J.; Goodwin, D. G. Growth on the Reconstructed Diamond (100) Surface. *J. Phys. Chem.* **1993**, *97*, 23−28.
(4) Butler, J. E.; Woodin, R. L.; Brown, L. M.; Fallon, P. Thin Film Diamond Growth Mechanisms. *Philos. Trans. R. Soc., A* **1993**, *342*, 209−224.
(5) Skokov, S.; Weiner, B.; Frenklach, M. Elementary Reaction Mechanism for Growth of Diamond (100) Surfaces from Methyl Radicals. *J. Phys. Chem.* **1994**, *98*, 7073−7082.
(6) Frenklach, M.; Skokov, S. Surface Migration in Diamond Growth. *J. Phys. Chem. B* **1997**, *101*, 3025−3036.
(7) Goodwin, D. G.; Butler, J. E. In *Handbook of Industrial Diamonds and Diamond Films;* Prelas, M., Popovici, G., Bigelow, L. G., Eds.; Marcel Dekker: New York, 1998; pp 527−581.
(8) Battaile, C. C.; Srolovitz, D. J.; Butler, J. E. Atomic Scale Simulations of Chemical Vapor Deposition on Flat and Vicinal Diamond Substrates. *J. Cryst. Growth* **1998**, *194*, 353−68.
(9) Larsson, K.; Carlsson, J. O. Surface Migration during Diamond Growth Studied by Molecular Orbital Calculations. *Phys. Rev. B: Condens. Matter Mater. Phys.* **1999**, *59*, 8315−8322.
(10) Battaile, C. C.; Srolovitz, D. J. Kinetic Monte Carlo Simulation of Chemical Vapor Deposition. *Annu. Rev. Mater. Res.* **2002**, *32*, 297−319.
(11) Netto, A.; Frenklach, M. Kinetic Monte Carlo Simulations of CVD Diamond Growth − Interplay among Growth, Etching and Migration. *Diamond Relat. Mater.* **2005**, *14*, 1630−1646.
(12) Cheesman, A.; Harvey, J. N.; Ashfold, M. N. R. Studies of Carbon Incorporation on the Diamond [100] Surface during Chemical Vapor Deposition using Density Functional Theory. *J. Phys. Chem. A* **2008**, *112*, 11436−11448.
(13) Richley, J. C.; Harvey, J. N.; Ashfold, M. N. R. On the Role of Carbon Radical Insertion Reactions in the Growth of Diamond by

DOI: 10.1021/acs.jpca.7b00466
J. Phys. Chem. A 2017, 121, 2046−2055

Chemical Vapor Deposition Methods. *J. Phys. Chem. A* **2009**, *113*, 11416−11422.
(14) Butler, J. E.; Mankelevich, Y. A.; Cheesman, A.; Ma, J.; Ashfold, M. N. R. Understanding the Chemical Vapor Deposition of Diamond: Recent Progress. *J. Phys.: Condens. Matter* **2009**, *21*, 364201.
(15) Mankelevich, Y. A.; Ashfold, M. N. R.; Ma, J. Plasma-Chemical Processes in Microwave Plasma-Enhanced Chemical Vapor Deposition Reactors Operating with C/H/Ar Gas Mixtures. *J. Appl. Phys.* **2008**, *104*, 113304.
(16) Cheesman, A.; Harvey, J. N.; Ashfold, M. N. R. Computational Studies of Elementary Steps Relating to Boron Doping During Diamond Chemical Vapour Deposition. *Phys. Chem. Chem. Phys.* **2005**, *7*, 1121−1126.
(17) Ma, J.; Richley, J. C.; Davies, D. R. W.; Ashfold, M. N. R.; Mankelevich, Y. A. Spectroscopic and Modeling Investigations of the Gas Phase Chemistry and Composition in Microwave Activated B_2H_6/CH_4/Ar/H_2 Mixtures. *J. Phys. Chem. A* **2010**, *114*, 10076−10089.
(18) Jin, S.; Moustakas, T. D. Effect of Nitrogen on theGrowth of Diamond Films. *Appl. Phys. Lett.* **1994**, *65*, 403−405.
(19) Locher, R.; Wild, C.; Herres, D.; Behr, D.; Koidl, P. Nitrogen Stabilized (100) Texture in Chemical Vapor Deposited Diamond Films. *Appl. Phys. Lett.* **1994**, *65*, 34−36.
(20) Müller-Sebert, W.; Wörner, E.; Fuchs, F.; Wild, C.; Koidl, P. Nitrogen Induced Increase of Growth Rate in Chemical Vapor Deposition of Diamond. *Appl. Phys. Lett.* **1996**, *68*, 759−760.
(21) Cao, G. Z.; Schermer, J. J.; van Enckevort, W. J. P.; Elst, W. A. L. M.; Giling, L. J. Growth of {100} Textured Diamond Films by the Addition of Nitrogen. *J. Appl. Phys.* **1996**, *79*, 1357−1364.
(22) Silva, F.; Gicquel, A. Structural Characteristics of CVD Diamond Films versus Nitrogen Impurities Coupled to other Deposition Parameters. *Electrochem. Soc. Proc.* **1998**, *97*, 99−125.
(23) Benedic, F.; Belmahi, M.; Elmazria, O.; Assouar, M. B.; Fundenberger, J. J.; Alnot, P. Investigations on Nitrogen Addition in the CH_4-H_2 Gas Mixture used for Diamond Deposition for a Better Understanding and the Optimisation of the Synthesis Process. *Surf. Coat. Technol.* **2003**, *176*, 37−49.
(24) Chayahara, A.; Mokuno, Y.; Horino, Y.; Takasu, Y.; Kato, H.; Yoshikawa, H.; Fujimori, N. The Effect of Nitrogen Addition During High-Rate Homoepitaxial Growth of Diamond by Microwave Plasma CVD. *Diamond Relat. Mater.* **2004**, *13*, 1954−1958.
(25) Tallaire, A.; Collins, A. T.; Charles, D.; Achard, J.; Sussmann, R.; Gicquel, A.; Newton, M. E.; Edmonds, A. M.; Cruddace, R. J. Characterisation of High-Quality Thick Single-Crystal Diamond by CVD with a Low Nitrogen Addition. *Diamond Relat. Mater.* **2006**, *15*, 1700−1707.
(26) Achard, J.; Silva, F.; Brinza, O.; Tallaire, A.; Gicquel, A. Coupled Effect of Nitrogen Addition and Surface Temperature on the Morphology and the Kinetics of Thick CVD Diamond Single Crystals. *Diamond Relat. Mater.* **2007**, *16*, 685−689.
(27) Dunst, S.; Sternschulte, H.; Schreck, M. Growth Rate Enhancement by Nitrogen in Diamond Chemical Vapor Deposition − A Catalytic Effect. *Appl. Phys. Lett.* **2009**, *94*, 224101.
(28) Yamada, H.; Chayahara, A.; Mokuno, Y. Effects of Intentionally Introduced Nitrogen and Substrate Temperature on Growth of Diamond Bulk Single Crystals. *Jpn. J. Appl. Phys.* **2016**, *55*, 01AC07.
(29) Van Regemorter, T.; Larsson, K. Effect of a NH Coadsorbate on the CH_3 (or CH_2) Adsorption to a Surface Step on Diamond (100). *J. Phys. Chem. C* **2009**, *113*, 19891−19896.
(30) Van Regemorter, T.; Larsson, K. A Theoretical Study of Nitrogen-Induced Effects on Initial Steps of Diamond CVD Growth. *Chem. Vap. Deposition* **2008**, *14*, 224−231.
(31) Van Regemorter, T.; Larsson, K. Effect of Substitutional N on Important Chemical Vapor Deposition Growth Steps. *J. Phys. Chem. A* **2009**, *113*, 3274−3284.
(32) Yiming, Z.; Larsson, F.; Larsson, K. Effect of CVD Diamond Growth by Doping with Nitrogen. *Theor. Chem. Acc.* **2014**, *133*, 1432.
(33) Butler, J. E.; Oleynik, I. A Mechanism for Crystal Twinning in the Growth of Diamond by Chemical Vapour Deposition. *Philos. Trans. R. Soc., A* **2008**, *366*, 295−311.
(34) Michl, J.; Teraji, T.; Zaiser, S.; Jakobi, I.; Waldherr, G.; Dolde, F.; Neumann, P.; Doherty, M. W.; Manson, N. B.; Isoya, J.; Wrachtrup, J. Perfect Alignment and Preferential Orientation of Nitrogen-Vacancy Centers during Chemical Vapor Deposition Diamond Growth on (111) Surfaces. *Appl. Phys. Lett.* **2014**, *104*, 102407.
(35) Lesik, M.; Tetienne, J. P.; Tallaire, A.; Achard, J.; Mille, V.; Gicquel, A.; Roch, J. F.; Jacques, V. Perfect Preferential Orientation of Nitrogen-Vacancy Defects in a Synthetic Diamond Sample. *Appl. Phys. Lett.* **2014**, *104*, 113107.
(36) Fukui, T.; Doi, Y.; Miyazaki, T.; Miyamoto, Y.; Kato, H.; Matsumoto, T.; Makino, T.; Yamasaki, S.; Morimoto, R.; Tokuda, N.; Hatano, M.; Sakagawa, Y.; Morishita, H.; Tashima, T.; Miwa, S.; Suzuki, Y.; Mizuochi, N. Perfect Selective Alignment of Nitrogen-Vacancy Centers in Diamond. *Appl. Phys. Express* **2014**, *7*, 055201.
(37) Miyazaki, T.; Miyamoto, Y.; Makino, T.; Kato, H.; Yamasaki, S.; Fukui, T.; Doi, Y.; Tokuda, N.; Hatano, M.; Mizuochi, N. Atomistic Mechanism of Perfect Alignment of Nitrogen-Vacancy Centers in Diamond. *Appl. Phys. Lett.* **2014**, *105*, 261601.
(38) Karin, T.; Dunham, S.; Fu, K.-M. Alignment of the Diamond Nitrogen Vacancy Center by Strain Engineering. *Appl. Phys. Lett.* **2014**, *105*, 053106.
(39) Bachmann, P. K.; Leers, D.; Lydtin, H. Towards a General Concept of Diamond Chemical Vapor-Deposition. *Diamond Relat. Mater.* **1991**, *1*, 1−12.
(40) Mollart, T. P.; Lewis, K. L. Optical-Quality Diamond Growth from CO_2-Containing Gas Chemistries. *Diamond Relat. Mater.* **1999**, *8*, 236−241.
(41) Richley, J. C.; Kelly, M. W.; Ashfold, M. N. R.; Mankelevich, Y. A. Optical Emission from Microwave Activated C/H/O Gas Mixtures for Diamond Chemical Vapor Deposition. *J. Phys. Chem. A* **2012**, *116*, 9447−9458.
(42) Kelly, M. W.; Richley, J. C.; Western, C. M.; Ashfold, M. N. R.; Mankelevich, Y. A. Exploring the Plasma Chemistry in Microwave Chemical Vapor Deposition of Diamond from C/H/O Gas Mixtures. *J. Phys. Chem. A* **2012**, *116*, 9431−9446.
(43) Truscott, B. S.; Kelly, M. W.; Potter, K. J.; Ashfold, M. N. R.; Mankelevich, Y. A. Microwave Plasma-Activated Chemical Vapor Deposition of Nitrogen Doped Diamond, II: CH_4/N_2/H_2 Plasmas. *J. Phys. Chem. A* **2016**, *120*, 8537−8549.
(44) Richley, J. C.; Harvey, J. N.; Ashfold, M. N. R. CH_2 Group Migration between H-Terminated 2 × 1 Reconstructed {100} and {111} Surfaces of Diamond. *J. Phys. Chem. C* **2012**, *116*, 7810−7816.
(45) Richley, J. C.; Harvey, J. N.; Ashfold, M. N. R. Boron Incorporation at a Diamond Surface: A QM/MM Study of Insertion and Migration Pathways During Chemical Vapor Deposition. *J. Phys. Chem. C* **2012**, *116*, 18300−18307.
(46) Frisch, M. J.; Trucks, G. W.; Schlegel, H. B.; Scuseria, G. E.; Robb, M. A.; Cheeseman, J. R.; Scalmani, G.; Barone, V.; Mennuchi, B.; Petersson, G.; et al. *Gaussian 09;* Gaussian Inc.: Pittsburgh, PA, 2009.
(47) Harvey, J. N. Spin-forbidden CO ligand recombination in myoglobin. *Faraday Discuss.* **2004**, *127*, 165−177.
(48) Tsipis, A. C.; Orpen, A. G.; Harvey, J. N. Substituent Effects and the Mechanism of Alkene Metathesis Catalyzed by Ruthenium Dichloride Catalysts. *Dalton Trans.* **2005**, 2849−2858.
(49) *Jaguar:* Rapid ab Initio Electronic Structure Package; Schrödinger Inc.: Portland, OR, 2000.
(50) Ponder, J. W. *TINKER:* Software Tools for Molecular Design, v 4.0; Washington University: Saint Louis, MO, 2003.
(51) Skokov, S.; Weiner, B.; Frenklach, M. Theoretical Study of Oxygenated (100) Diamond Surfaces in the Presence of Hydrogen. *Phys. Rev. B: Condens. Matter Mater. Phys.* **1997**, *55*, 1895−1901.
(52) Tamura, H.; Zhou, H.; Sugisako, K.; Yokoi, Y.; Takami, S.; Kubo, M.; Teraishi, K.; Miyamoto, A.; Imamura, A.; N.-Gamo, M.; Ando, T. Periodic Density-Functional Study of Oxidation of Diamond (100) Surfaces. *Phys. Rev. B: Condens. Matter Mater. Phys.* **2000**, *61*, 11025−11033.

DOI: 10.1021/acs.jpca.7b00466
J. Phys. Chem. A 2017, 121, 2046−2055

(53) Tamura, H.; Zhou, H.; Takami, S.; Kubo, M.; Miyamoto, A.; N.-Gamo, M. N.; Ando, T. Effect of S and O on the Growth of Chemical-Vapor Deposited Diamond (100) Surfaces. *J. Chem. Phys.* **2001**, *115*, 5284−5291.
(54) Ando, T.; Yamamoto, K.; Ishii, M.; Kamo, M.; Sato, Y. Vapour-phase Oxidation of Diamond Surfaces in O_2 Studied by Diffuse Reflectance Fourier-transform Infrared and Temperature-programmed Desorption Spectroscopy. *J. Chem. Soc., Faraday Trans.* **1993**, *89*, 3635−3640.
(55) Hossain, M. Z.; Kubo, T.; Aruga, T.; Takagi, N.; Tsuno, T.; Fujimori, N.; Nishijima, M. Chemisorbed States of Atomic Oxygen and its Replacement by Atomic Hydrogen on the Diamond (100)-(2′1) Surface. *Surf. Sci.* **1999**, *436*, 63−71.
(56) Petrini, D.; Larsson, K. A Theoretical Study of the Energetic Stability and Geometry of Hydrogen- and Oxygen-Terminated Diamond (100) Surfaces. *J. Phys. Chem. C* **2007**, *111*, 795−801.

DOI: 10.1021/acs.jpca.7b00466
J. Phys. Chem. A 2017, 121, 2046−2055